

Observation of the full spiral spectrum of a light beam with single-pixel detection

LUIS JOSÉ SALAZAR-SERRANO¹, JOB MENDOZA-HERNÁNDEZ¹, JUAN P. TORRES^{1,2}

¹ICFO - The Institute of Photonic Sciences, the Barcelona Institute of Science and Technology
08860 Castelldefels (Barcelona), Spain

²Dep. Signal Theory and Communications, Universitat Politècnica de Catalunya
Campus Nord D3, 08034 Barcelona, Spain

Corresponding author: juanp.torres@icfo.eu

November 6, 2018

We demonstrate experimentally a *simple* and *easy-to-use* technique aimed at measuring the complex orbital angular momentum spectrum of an arbitrary optical field making use of just polarization measurements. The technique can be applied to any other family of modes used to describe the spatial shape of optical beams. The idea is inspired by a formal analogy that exist between classical fields that can show certain amount of correlations between different degrees of freedom (polarization and spatial shape) and the degree of entanglement that might exist between two subsystems, so it is an example of a *quantum-inspired* classical technology.

1. INTRODUCTION

Tailoring of the the spatial shape of light beams is an important resource that is being considered nowadays for many novel photonic applications [1, 2]. In general, the spatial shape cannot be considered separately from the polarization (spin) [3, 4]. However, in the paraxial regime both contributions can be measured and manipulated independently, so the description of the spatial shape of a light beam can be considered separately from its polarization.

In this scenario, the spatial distribution of the intensity and phase of the optical field, $F(x, y)$, even down to the single photon limit, can be written as a mode decomposition

$$F(x, y) = \sum_m C_m G_m(x, y), \quad (1)$$

where $C_m = \int dx dy F(x, y) G_m^*(x, y)$, $G_m(x, y)$ is a set of functions that constitute a basis and the array $\{C_m\}$ is the set of complex numbers that uniquely describe $F(x, y)$.

In many applications [5, 6, 7] one chooses as basis the set of Laguerre-Gauss modes, $\varphi_{l,p}(x, y)$, where the modes are labeled by two indexes $m = l, p$ and each mode carries an orbital angular momentum (OAM) of

$m\hbar$ per photon [9]. In this case, the array $\{C_{lp}\}$ is the so-called spiral spectrum of the light beam [8]. Notwithstanding, a family of modes might exist that is more convenient to describe the optical field transformations that take place, by and large.

In principle, we can think of obtaining full information about the spatial shape of the beam, amplitude and phase of the optical field at each point, by measuring these quantities directly with a variety of methods available that require the use of a CCD camera. Afterwards one can calculate any mode decomposition of the optical field computationally. For instance, phase-shifting digital holography [10] measures the spatial shape of the optical field by measuring the intensity resulting from the interference of the field with a reference field with four different phase offsets.

However, these types of procedures based on the use of *multiple pixels* (cameras) might not be very convenient in most practical applications. This is especially true at wavelengths where there are no good cameras or these are complicated, bulky and expensive [11]. In this scenario it might be preferable to measure directly the weights of the corresponding mode decomposition, or the weights of specific modes of interest, which can be done with the help of a single-pixel camera. This

would make easier the measurement of optical fields at wavelengths where mega-pixel cameras are not affordable.

There are also applications where the information of interest about an object can be retrieved observing specific modes contained in the optical field. This is the case, for instance of Digital Spiral Imaging [12, 13], where one aims at probing certain properties of a sample by inspecting how certain spatial modes are transformed by its interaction with the sample. In this case it seems indeed unnecessary to obtain full information of the field.

Several techniques aimed at elucidating the orbital angular momentum spectrum of arbitrary optical fields has been put forward and demonstrated over the years. Vasnetsov et al. [14] showed that the OAM spectrum of light beams can be retrieved measuring the different frequency shifts induced by the rotation of each OAM mode contained in the field around the beam axis [15, 16]. However rotating a beam about its own axis at a fast rate is generally difficult.

One can concatenate interferometers that sort out different OAM states, although due to its interferometric nature this technique is technically demanding [17]. Another approach is to make use of a technique that transforms helically phase beams to tilted plane waves, where the tilt depends on the OAM index, and then measure the intensity at different positions with the help of a CCD camera [18]. With a similar technique Trichili et al. [19] were able to identify with high fidelity 105 encoded modes where each mode manifest as separate spatial locations after transmission through a properly engineered transmission filter.

By projecting the incoming optical field into a specific mode $\varphi_{l,p}(x,y)$, with the help of holograms or computer-controlled spatial light modulators (SLM), and detecting the outgoing intensity, one can measure the OAM spectrum $\{|C_m|^2\}$. Notice that this method provides no information about the phase of the spectrum, which may be relevant in certain applications. The measurement of the phase necessitates projecting into combinations of modes [20].

One drawback of these projection-based measurements is that one needs to perform a sequence of projective measurements at different times, hence the time to characterize an optical field increases with the dimension of its modal spectrum, which makes difficult the measurement of fields with large dimensions. Recently a technique aimed at overcoming this limitation and

that performs direct measurements of complex fields with extremely high dimensionality have been demonstrated [21, 22].

Here we put forward and demonstrate a *simple* scheme to measure the full complex spectrum of an arbitrary optical field. The idea (see Fig. 1) is to generate, with the help of a polarizing beam splitter, a combined state of polarization and spatial shape of the form $\Psi(x,y) = F(x,y)\mathbf{H} + G_m(x,y)\mathbf{V}$, and perform only polarization measurements of the outgoing signal. $F(x,y)$ is the optical field to be characterized, $G_m(x,y)$ is the basis and \mathbf{H} and \mathbf{V} designate horizontal and vertical polarizations, respectively.

The technique described here is a clear example of how quantum insights can inspire novel classical technologies. The idea of our technique comes from noticing the similarity of the classical field

$$\Psi(x,y) = F(x,y)\mathbf{H} + G(x,y)\mathbf{V}, \quad (2)$$

with the quantum state of a single photon [23, 24, 25]

$$|\Psi\rangle = \frac{1}{\sqrt{2}} \left[a_{f,\mathbf{H}}^\dagger + a_{g,\mathbf{V}}^\dagger \right] |vac\rangle, \quad (3)$$

where $a_{f,\mathbf{H}}^\dagger$ is the creation operator of a photon with spatial shape $f(x,y)$ and horizontal polarization; similarly $a_{f,\mathbf{V}}^\dagger$ is the creation operator for a photon with spatial shape $g(x,y)$ and vertical polarization.

If one would apply the quantum concepts of purity and concurrence [26] to the states given by Eqs. (2) or (3), the purity would read as

$$P = (1 + |\epsilon|^2)/2, \quad (4)$$

and the concurrence

$$C = |\epsilon|, \quad (5)$$

where

$$\epsilon = \int dx dy F(x,y)G^*(x,y), \quad (6)$$

is the overlap between the fields F and G . In this scenario of formal similarities, the entropy of entanglement would read as

$$S = -\lambda_1 \log_2 \lambda_1 - \lambda_2 \log_2 \lambda_2, \quad (7)$$

where

$$\lambda_{1,2} = \frac{1}{2} (1 \pm |\epsilon|). \quad (8)$$

If F and G are orthogonal there is maximum *entanglement* of 1 ebit, and the polarization state is an incoherent combinations of vertical and horizontal polarization.

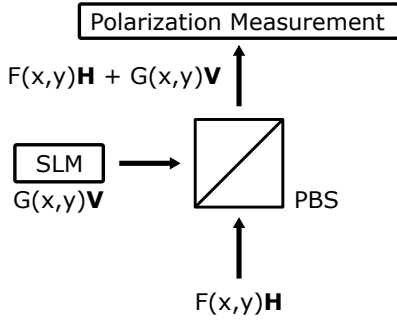


Figure 1: Sketch of the technique aimed at measuring the complex overlap between two light beams with spatial profiles $F(x,y)$ and $G(x,y)$. The input beam with spatial profile $F(x,y)$ and horizontal polarization is combined with a second beam with vertical polarization and spatial profile $G(x,y)$. The state of polarization of the outgoing signal is measured, which gives the sought-after overlap between both functions.

If they are almost equal, the entanglement is close to zero and the state of polarization is $1/\sqrt{2}(\mathbf{H} + \mathbf{V})$. We make use these *quantum-classical* formal analogies to devise a technique to obtain the complex OAM spectrum of an arbitrary optical field with just polarization measurements.

2. THEORETICAL BACKGROUND

The scheme, described by Fig.1, is implemented experimentally by embedding the optical field of interest $F(x,y)$ with horizontal polarization and generating with an SLM a family of modes $G_m(x,y)$ that constitute a basis to describe an arbitrary optical field. The modes of the basis show vertical polarization. The outgoing signal $\Psi(x,y)$ after the polarizing beam splitter (PBS) is given by Eq. (2), and can be written as

$$\Psi(x,y) = \frac{\mathbf{D} + \mathbf{A}}{\sqrt{2}}F(x,y) + \frac{\mathbf{D} - \mathbf{A}}{\sqrt{2}}G_m(x,y), \quad (9)$$

where the diagonal polarization reads as $\mathbf{D} = (\mathbf{H} + \mathbf{V})/\sqrt{2}$ and the anti-diagonal polarization reads as $\mathbf{A} = (\mathbf{H} - \mathbf{V})/\sqrt{2}$. The power detected when the outgoing signal is projected into the \mathbf{D} and \mathbf{A} polarization states are

$$P_D = \frac{1}{2} [I_F + I_{G_m} + 2\mathcal{R}(C_m)],$$

$$P_A = \frac{1}{2} [I_F + I_{G_m} - 2\mathcal{R}(C_m)],$$

where \mathcal{R} designates the real part. Therefore,

$$\mathcal{R}(C_m) = \frac{P_D - P_A}{2}. \quad (10)$$

Similarly, if we project the signal into circularly-polarized polarization states $\mathbf{R} = (\mathbf{H} + i\mathbf{V})/\sqrt{2}$ and $\mathbf{L} = (\mathbf{H} - i\mathbf{V})/\sqrt{2}$,

$$P_R = \frac{1}{2} [I_F + I_{G_m} - 2\mathcal{I}(C_m)],$$

$$P_L = \frac{1}{2} [I_F + I_{G_m} + 2\mathcal{I}(C_m)], \quad (11)$$

where \mathcal{I} designates the imaginary part. Finally we obtain

$$\mathcal{I}(C_m) = \frac{P_L - P_R}{2}. \quad (12)$$

Notice that we measure $\mathcal{R}(C_m)$ and $\mathcal{I}(C_m)$ by performing polarization measurements only. One can thus take advantage of the enormous set of high-quality optical components existing aimed at manipulating and measuring optical polarization.

3. EXPERIMENTAL RESULTS

3.1. Experimental scheme

The experimental scheme is shown in figure 2. A He-Ne laser (Melles Griot, $\lambda = 632.8\text{nm}$) generates a Gaussian beam polarized at $+45^\circ$ with the help of a Half Wave Plate, HWP_1 . Afterwards, the beam is split into two beams that propagate parallel and that are spatially separated a distance d , by means of a Tunable Beam Displacer [27], TBD_1 . The TBD is a device composed of a Polarizing Beam Splitter (PBS) and an L-shaped platform with two fixed mirrors arranged in a Sagnac like configuration. The platform is free to rotate with respect to the PBS center with the help of a standard rotating stage. When the platform is rotated at a certain angle θ , an input beam polarized at $+45^\circ$ is divided into two parallel beams whose separation can be continuously tuned (i.e. $d \propto \theta$). The two output beams are linearly polarized with either horizontal or vertical polarization and no optical path difference is introduced between them. The wavelength dependence of the TBD, the maximum separation between the output beams and its spatial quality are mainly determined by the PBS characteristics.

The two output beams leaving TBD_1 impinge on different areas of the Spatial Light Modulator (SLM). The

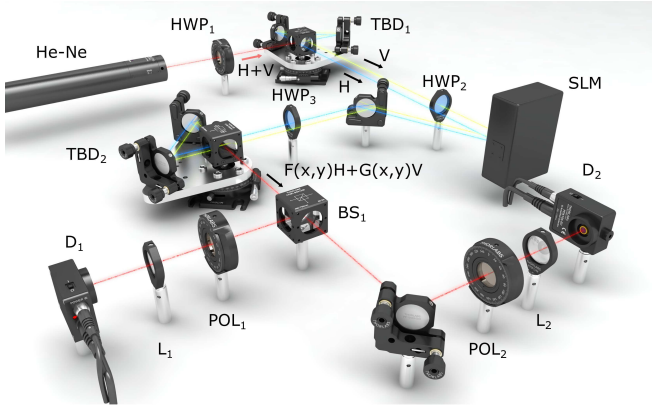


Figure 2: Experimental scheme. An input beam with Gaussian profile is split spatially into two beams with orthogonal polarizations (TBD₁). The beams with horizontal and vertical polarizations acquire different spatial beam profile given by $F(x, y)$ and $G_m(x, y)$, respectively, by means of a SLM. After combining (TBD₂) the beams and performing a polarization measurement, the overlap between $F(x, y)$ and $G_m(x, y)$ is measured. HWP: Half-Wave plate; TBD: Tunable Beam Displacer; SLM: Spatial Light Modulator; BS: Beam Splitter (50:50); POL: Polarizer; L: Lens; D: detector.

screen of the SLM is divided into two separate sections that imprint a different spatially varying phase after reflection to each incoming beam. In Fig. 2, the rightmost section introduces a phase profile so that the output beam spatial beam profile is described by the function $F(x, y)$. Similarly, the left section generates a beam described by the function $G_m(x, y)$. Notice that since the SLM can only operate on input beams with horizontal polarization, a second Half Wave Plate, HWP₂, is introduced before the SLM in the path of one of the incoming beams in order to rotate its polarization from vertical to horizontal and impinge on the SLM with the required polarization.

After the SLM, TBD₂ combines the two spatially separated beams into a single beam. In order to guarantee that the second TBD operates in inverse mode (with respect to TBD₁) the polarization state of one of the input beams is rotated by 90°, by a third HWP (HWP₃) so that two input beams separated by a distance d and with orthogonal polarizations are the input. After TBD₂, the output beam is composed of two collinear beams with orthogonal polarizations. At this point, the optical field

reads

$$\Psi(x, y) = F(x, y) \mathbf{H} + G_m(x, y) \exp(i\phi) \mathbf{V}, \quad (13)$$

where ϕ is a phase introduced by the SLM aimed at i) compensating any unwanted phase due to misalignment and ii) it allows to measure the imaginary part of C_m by replacing ϕ for $\phi + \pi/2$.

In order to measure the real part of the overlap C_m , the optical signal is divided in two components with equal amplitudes. One component is projected into a diagonal (\mathbf{D}) polarization state and the other into an anti-diagonal (\mathbf{A}) polarization state. After projection, the power measurements of detectors D₁ and D₂ are subtracted. In the experiment, measurements are performed by two detectors Thorlabs PDA36A-EC connected to a NI-USB 6009 data acquisition card. The whole measurement procedure is controlled using a Python script that generates for each SLM window a set of phase masks that describe the functions $F(x, y)$ and $G_m(x, y)$, varies the phase ϕ , performs the power measurements and records the data obtained.

Following a similar procedure, the imaginary component of C_m is measured after adding a phase of $\pi/2$ to the current value of ϕ . This is achieved by increasing the minimum gray level on the left window of the SLM. In order to measure the full spiral spectrum of the beam described by the function $F(x, y)$, two sets of measurements are performed. In the first set, the real part is determined and is recorded as a function of the basis index m corresponding to $G_m(x, y)$. In the second set, the imaginary part is measured by performing the same scan over the index m after adding $\pi/2$ to ϕ . The whole measurements provides information about the complex character of $\{C_m\}$.

3.2. Results

In order to validate the technique described here, we consider different optical fields $F(x, y)$ and measure its overlap (C_l) with a set of LG modes with $p = 0$. As a first example, Fig. 3 considers the decomposition of a LG beam with OAM index $l = -3$ and varying phase ϕ , i.e., $F(x, y) = \varphi_{l=-3}(x, y) \exp(i\phi)$, in terms of 21 LG modes with $l \in [-10, 10]$. Figs 3(a) to 3(d) depict the real and imaginary parts of C_l for (a) $\phi = 3.92$, (b) $\phi = 0.78$, (c) $\phi = 5.49$ and (d) $\phi = 2.35$. The data recorded shows a peak centered in $l = -3$, as expected and the amplitude of the real and imaginary components, indicated by the red and blue bars respectively, varies according to the phase ϕ as expected.

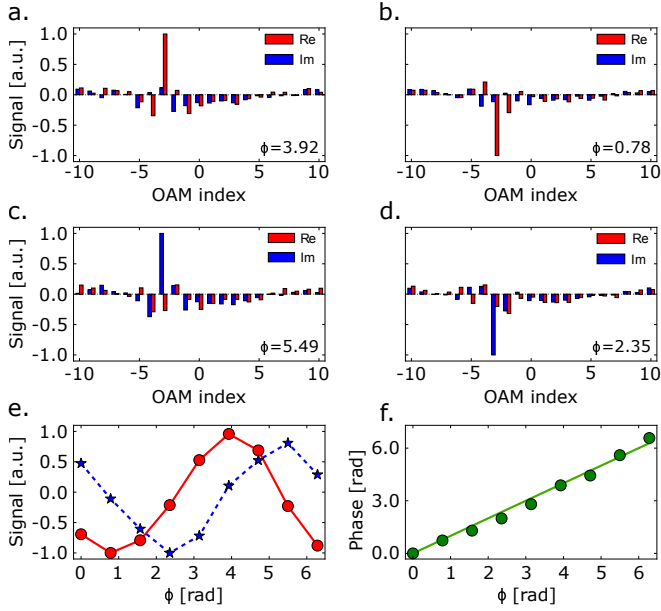


Figure 3: Spiral spectrum of a LG beam with OAM index $l=-3$ (see text for details). Notice the change of sign of the signal in panels (a) - (b), and panels (c) - (d), due to the different choice of the phase ϕ . In (e) we show the real (dots) and imaginary (stars) parts of the overlap function $C_{l=-3}$ as a function of ϕ for $[0, 2\pi]$. (f) shows the phase of C_l obtained from the curves in (e) (dots: experiment; line: theory).

However the main peak is accompanied by other minor peaks at $l \neq -3$ with small amplitudes. These secondary peaks appear due to the fact that the spatial modes at the output of TBD_2 are not pure LG modes. The PBS present in each TBD degrades significantly the spatial quality of any input beam. In particular, we have noticed that the spatial quality of the reflected LG beams varies significantly with respect to the transmitted counterpart.

In addition to this, the amplitude of these secondary peaks is also related to the quality of the 50 : 50 beam splitter BS_1 positioned after TBD_2 . Since the reflected and transmitted components are not split equally, the first and second terms of P_R and P_L in Eq. (11) does not fully cancel after subtraction. As an example, for the BS used in the experiment (Thorlabs pellicle BS CM1-BP150), the reflected component with horizontal polarization has an amplitude reduction of 10% to 20% with respect to the other beams, namely, reflected beam with vertical polarization and transmitted beam with horizontal and vertical polarizations.

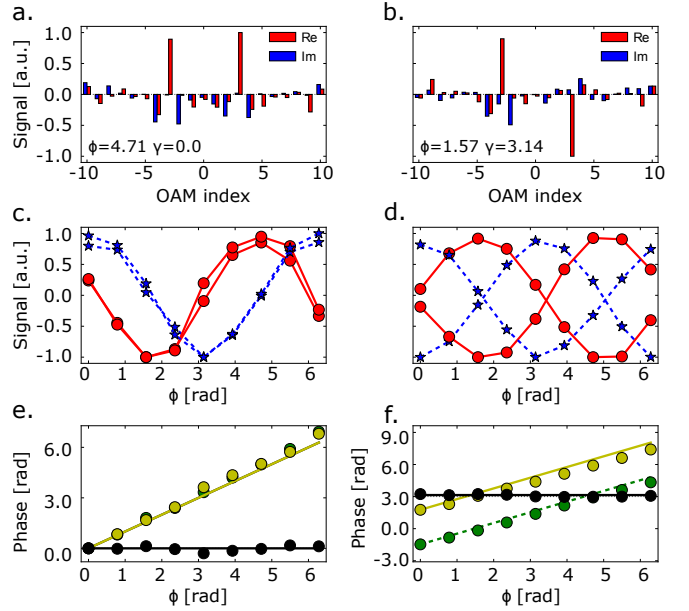


Figure 4: Spiral spectrum of a superposition of two LG beams with OAM indexes $l = +3$ and $l = -3$. (a), (c) and (e): the two LG beams have the same phase ($\gamma = 0$), and (b), (d) and (f): the two LG beams have a relative phase of $\gamma = \pi$. (c) and (d) show the real (dots) and imaginary (stars) parts of the overlap functions $C_{l=-3}$ and $C_{l=+3}$ as a function of ϕ for $[0, 2\pi]$. (e) depicts the phase as a function of ϕ and the phase difference between mode projections. Notice that, even though ϕ increases, the difference remains zero as expected (black line). Similarly, (f) shows the phase of each overlap function when $\gamma = \pi$. In this case, the black line indicates a difference in phase of ~ 3.14 , as expected (dots:experiment; lines: theory).

Fig. 3(e) shows the real (circles) and imaginary (stars) parts of the signal measured as a function of the varying phase ϕ . Notice that even though $F(x, y)$ and $G_l(x, y)$ are real functions, the measured real component is maximum for a non-zero phase due to the fact that an additional phase is introduced due to misalignments on the TBDs. Finally Fig. 3(f) shows the phase calculated from the real and imaginary values measured in Fig. 3(e), as a function of the phase ϕ . The continuous line indicates the expected phase measured as a function of the phase introduced by the SLM experimentally.

Fig. 4 presents experimental results for a more general case where the optical fields is $F(x, y) \sim [\varphi_{l=+3}(x, y) + \exp(i\gamma)\varphi_{l=-3}(x, y)] \exp(i\phi)$, where γ

corresponds to a relative phase between the two modes. Figs. 4(a) and (b) present the measured overlap C_l for two selected cases. In both cases, two main peaks centered at $l = -3$ and $l = +3$ are observed. For $\phi = 4.71$ (Fig. 4(a)), the real part of $C_{l=+3}$ is maximum. The peaks corresponding to $l = -3$ and $l = +3$ have the same sign and very similar amplitude. Fig. 4(c) shows the overlaps $C_{l=-3}$ and $C_{l=+3}$ measured (real and imaginary parts) as a function of the phase ϕ . The phases of $C_{l=-3}$ and $C_{l=+3}$ are plotted in Fig. 4(e). As expected, since $\gamma = 0$, although the phases of $C_{l=-3}$ and $C_{l=+3}$ varies as $\sim \exp(i\phi)$, the relative phase between both overlaps functions is zero (horizontal line).

To illustrate the capability of the technique presented, Fig. 4(b), (d) and (f) present the corresponding results for $\gamma = \pi$. Fig. 4(b) shows that $C_{l=-3}$ and $C_{l=+3}$ have opposite signs. Fig. 4(f) shows the measured phases of $C_{l=-3}$ and $C_{l=+3}$ as well as its difference. The plot confirms that the phase difference between modes $\varphi_{l=+3}$ and $\varphi_{l=-3}$ (horizontal line) is around 3.1 rad, which corresponds to π .

4. CONCLUSIONS

We have demonstrated a technique that allows to measure the complex mode spectrum of an arbitrary optical field with just polarization measurements. The technique, *simple* and *easy-to-use*, retrieves the real and imaginary parts of the overlap of the optical field under investigation with all the modes of the basis.

In order to obtain the full mode spectrum, the technique should scan sequentially all the modes of the basis, which can be time consuming when analyzing optical fields with very high dimensionality. However, new technological advances should appear [28] that might increase substantially the refreshing time of spatial light modulators, reducing therefore the time required to obtain the spectrum.

Finally, we notice that this technique is an example of how quantum insights can inspire novel classical technologies. The idea presented and demonstrated comes from noticing the formal similarity existing between classical fields that might show correlations between degrees of freedom and the tunable degree of entanglement that might exist between two quantum subsystems.

FUNDING INFORMATION

We acknowledge financial support from the Spanish Ministry of Economy and Competitiveness through the Severo Ochoa Programme for Centres of Excellence in R&D (SEV- 2015-0522) and from Fundació Privada Cellex. J. P. T. acknowledges support from the program ICREA Academia (Generalitat de Catalunya). J. M. H. acknowledges support from the Consejo Nacional de Ciencia y Tecnología (México).

REFERENCES

- [1] J. P. Torres and L. Torner, *Twisted Photons: Applications of Light with Orbital Angular Momentum*, Wiley-VCH 1st edition (2011).
- [2] Halina Rubinsztein-Dunlop et al., "Roadmap on structured light", *J. Optics* **19**, 013001 (2017).
- [3] J. D. Jackson, *Classical Electrodynamics*, John Wiley and sons, New York (1999).
- [4] C. Cohen-Tannoudji, J. Dupont-Roc, and G. Grynberg, *Photons and Atoms: Introduction to Quantum Electrodynamics*, John Wiley and sons, New York (1989).
- [5] J. Wang, J-Y. Yang, I. M. Fazal, N. Ahmed, Y. Yan, H. Huang, Y. Ren, Y. Yue, S. Dolinar, M. Tur and A. E. Willner, "Terabit free-space data transmission employing orbital angular momentum multiplexing", *Nat. Photonics* **6**, 488 (2012).
- [6] M. Hendrych, R. Gallego, M. Micuda, N. Brunner, A. Acin and J. P. Torres, "Experimental estimation of the dimension of classical and quantum systems", *Nat. Physics* **8**, 588 (2012).
- [7] X-L. Wang, X-D. Cai, Z-E. Su, M-C. Chen, D. Wu, L. Li, N-L. Liu, C-Y. Lu and J. W. Pan, "Quantum teleportation of multiple degrees of freedom of a single photon", *Nature* **518**, 516 (2015).
- [8] J. P. Torres, A. Alexandrescu, and Lluís Torner, "Quantum spiral bandwidth of entangled two-photon states", *Phys. Rev. A* **68**, 050301(R) (2003).
- [9] L. Allen, M. W. Beijersbergen, R. J. C. Spreeuw, and J. P. Woerdman, "Orbital angular momentum of light and the transformation of Laguerre-Gaussian laser modes", *Phys. Rev. A* **45**, 8185 (1992).

-
- [10] I. Yamaguchi and T. Zhang, "Phase-shifting digital holography", *Opt. Lett.* **22**, 1268 (1997).
- [11] M. F. Duarte, M. A. Davenport, D. Takhar, J. N. Laska, T. Sun, K. F. Kelly and R. G. Baraniuk, "Single-pixel imaging via compressive sampling," *IEEE Signal Processing Magazine* **25**, 83 (2008).
- [12] L. Torner, J. P. Torres, and S. Carrasco, "Digital spiral imaging", *Opt. Express* **13**, 873 (2005).
- [13] G. Xie, H. Song, Z. Zhao, G. Milione, Y. Ren, C. Liu, R. Zhang, C. Bao, L. Li, Z. Wang, K. Pang, D. Starodubov, M Tur, and A. E. Willner, "Using a Complex Optical Orbital-Angular-Momentum Spectrum to Measure Object Parameters: A Spatial Domain Approach", arXiv:1705.09051 (2017).
- [14] M. V. Vasnetsov, J. P. Torres, D. V. Petroc and L. Torner, "Observation of the orbital angular momentum spectrum of a light beam", *Opt. Lett.* **28**, 2285 (2003).
- [15] J. Courtial, D. A. Robertson, K. Dholakia, L. Allen, and M. J. Padgett, "Rotational Frequency Shift of a Light Beam", *Phys. Rev. Lett.* **81**, 4828 (1998).
- [16] H-L. Zhou, D-Z. Fu, J-J. Dong, D-X. Chen, X-L. Cai, F-L. Li and X-L. Zhang, "Orbital angular momentum complex spectrum analyzer for vortex light based on the rotational Doppler effect", *Light Science and Applications* **6**, e16251 (2017).
- [17] J. Leach, M. J. Padgett, S. M. Barnett, S. Franke-Arnold, and J. Courtial, "Measuring the Orbital Angular Momentum of a Single Photon", *Phys. Rev. Lett.* **88**, 257901 (2002).
- [18] G. C. G. Berkhout, M. P. J. Lavery, J. Courtial, M. W. Beijersbergen and M. J. Padgett, "Efficient sorting of orbital angular momentum states of light", *Phys. Rev. Lett.* **105**, 153601 (2010).
- [19] A. Trichili, C. Rosalez-Guzman, A. Dudley, B. Ndagano, A. B. Salem, M. Zghal and A. Forbes, "Optical communications beyond orbital angular momentum", *Scientific Reports* **6**, 27674 (2016).
- [20] C. Schulze, A. Dudley, D. Flamm, M. Duparre and A. Forbes, "Measurement of the orbital angular momentum density of light by modal decomposition", *New J. Phys.* **15**, 073025 (2013).
- [21] M. Malik, M. Mirhosseini, M. P. J. Lavery, J. Leach, M. J. Padgett and R. W. Boyd, "Direct measurement of a 27-dimensional orbital angular momentum state vector", *Nat. Comm.* **5**, 3115 (2014).
- [22] Z. Shi, M. Mirhosseini, J. Margiewicz, M. Malik, F. Rivera and R. W. Boyd, "Direct measurement of an one-million-dimensional photonic state", arXiv:1503.04713v1 (2015).
- [23] A. Valles, V. D'Ambrosio, M. Hendrych, M. Micuda, L. Marrucci, F. Sciarrino, and J. P. Torres, "Generation of tunable entanglement and violation of a Bell-like inequality between different degrees of freedom of a single photon", *Phys. Rev A* **90**, 052326 (2014).
- [24] E. Nagali, F. Sciarrino, F. De Martini, L. Marrucci, B. Piccirillo, E. Karimi and E. Santamato, "Quantum information transfer from spin to orbital angular momentum of photons", *Phys. Rev. Lett.* **103**, 013601 (2009).
- [25] E. Karimi, J. Leach, S. Slussarenko, B. Piccirillo, L. Marrucci, L. Chen, W. She, S. Franke-Arnold, M. J. Padgett and E. Santamato, "Spin-orbit hybrid entanglement of photons and quantum contextuality", *Phys. Rev. A* **82**, 022115 (2010).
- [26] W. K. Wootters, "Entanglement of formation of an arbitrary state of two qubits", *Phys. Rev. Lett.* **80**, 2245 (1998).
- [27] L. J. Salazar-Serrano, A. Valencia, and J. P. Torres, "Tunable beam displacer", *Rev. of Scientific Instruments* **86**, 033109 (2015).
- [28] Spatial Light modulators based on nematic Liquid Crystals on Silicon (LCOS) are too slow. Ferroelectric LCOS show a greater speed. For instance, Forth Dimension Displays (<http://www.forthdd.com>) offers a highly reflective Ferroelectric Liquid Crystal on Silicon (FLCoS) device with a very high switching speed of the ferroelectric liquid crystal ($< 50\mu\text{s}$), that enables rapid light modulation.